AD-A174 433 VIBRATION CONTROL IN ROTATING MACHINERY USING VARIABLE DYNAMIC STIFFNESS..(U) NORTH STAFFORDSHIRE POLYTECHNIC STAFFORD (ENGLAND) DEPT OF ME.. M J GOODWIN ET AL. 1/1

UNCLASSIFIED MAR 86 AFOSR-TR-86-1098-VOL-2 AFOSR-84-0360 F/G 13/9 NL

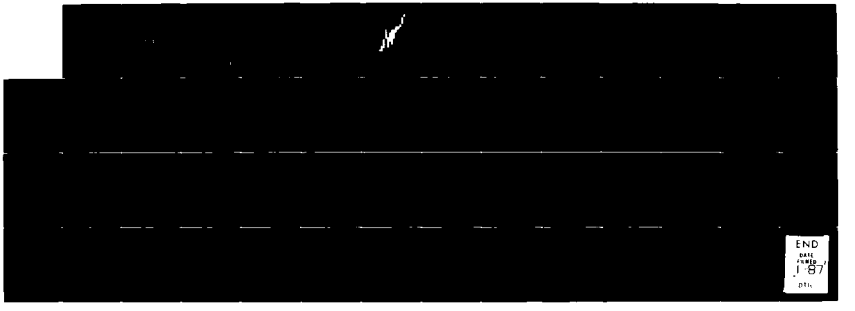

END
DATE FILMED
1-87
DTIC

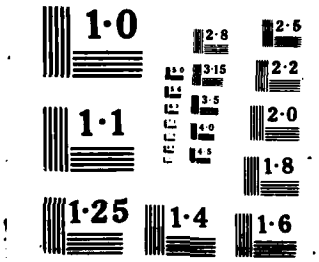
1·0
1·1
1·25
2·8
3·15
3·5
4·0
4·5
2·5
2·2
2·0
1·8
1·4
1·6

(2)

AFOSR-TR- 86-1098

AD-A174 433

# Vibration Control In Rotating Machinery Using Variable Dynamic Stiffness Squeeze Films

1st Full Interim Scientific Report
Covering the period Sept 1984 - Mar 1986
Volume 2

M J Goodwin, M P Roach

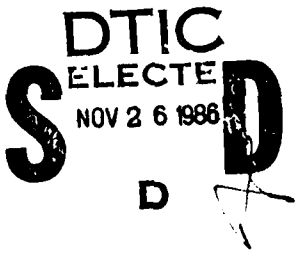

UNCLASSIFIED
SECURITY CLASSIFICATION OF THIS PAGE

## REPORT DOCUMENTATION PAGE

| | |
|---|---|
| 1a REPORT SECURITY CLASSIFICATION<br>Unclassified | 1b RESTRICTIVE MARKINGS |
| 2a SECURITY CLASSIFICATION AUTHORITY | 3 DISTRIBUTION / AVAILABILITY OF REPORT<br>Approved for public release:<br>Distribution unlimited |
| 2b DECLASSIFICATION / DOWNGRADING SCHEDULE | |
| 4 PERFORMING ORGANIZATION REPORT NUMBER(S) | 5 MONITORING ORGANIZATION REPORT NUMBER(S)<br>AFOSR-TR- 86-1098 |
| 6a NAME OF PERFORMING ORGANIZATION<br>North Staffordshire Polytechnic<br>6b OFFICE SYMBOL (If applicable) | 7a NAME OF MONITORING ORGANIZATION<br>European Office of Aerospace Research and Development/LTS |
| 6c ADDRESS (City, State, and ZIP Code)<br>Department of Mechanical and Computer-Aided Engineering<br>Beaconside, Stafford ST18 0AD, United Kingdom | 7b ADDRESS (City, State, and ZIP Code)<br>Box 14<br>FPO New York 09510-0200 |
| 8a NAME OF FUNDING / SPONSORING ORGANIZATION Air Force Office of Scientific Research<br>8b OFFICE SYMBOL (If applicable)<br>NA | 9 PROCUREMENT INSTRUMENT IDENTIFICATION NUMBER<br>AFOSR 84-0368 |
| 8c ADDRESS (City, State, and ZIP Code)<br>Bolling AFB, DC 20332-6448 | 10 SOURCE OF FUNDING NUMBERS<br>PROGRAM ELEMENT NO: 61102F; PROJECT NO: 2302; TASK NO: B1; WORK UNIT ACCESSION NO: |

11 TITLE (Include Security Classification)
VIBRATION CONTROL IN ROTATING MACHINERY USING VARIABLE DYNAMIC STIFFNESS SQUEEZE FILMS
VOLS [redacted] II

12 PERSONAL AUTHOR(S)
DR. M. J. GOODWIN AND M. P. ROACH

| 13a TYPE OF REPORT | 13b TIME COVERED | 14 DATE OF REPORT (Year, Month, Day) | 15 PAGE COUNT |
|---|---|---|---|
| ANNUAL | FROM Sep 84 TO Mar 86 | 1986 March | 50 |

16 SUPPLEMENTARY NOTATION

| 17 COSATI CODES | | |
|---|---|---|
| FIELD | GROUP | SUB-GROUP |
| | | |

18 SUBJECT TERMS (Continue on reverse if necessary and identify by block number)
Bearing, Squeeze Film, Vibration, Rotors

19 ABSTRACT (Continue on reverse if necessary and identify by block number)

This report describes the current status of a research project whose aim is to develop a hydrostatic bearing, for rotating machinery, whose dynamic characteristics may be tuned during operation of the machine. The purpose of this is to enable the operator to exercise some control over machine critical speeds and vibrations.

A computer program has been written which will predict both the static and dynamic characteristics of a hydrostatic bearing. The program allows for the presence of accumulators linked to the hydrostatic bearing recesses via flow restrictors. Output from the computer program has been used as input data to a second computer program which calculates machine vibration amplitude variation with running speed. Theoretical machine characteristics obtained in this way have been used to aid the design of a test rig which will be used to examine the practical performance of the new bearing type being developed.

| 20 DISTRIBUTION / AVAILABILITY OF ABSTRACT | 21 ABSTRACT SECURITY CLASSIFICATION |
|---|---|
| ☐ UNCLASSIFIED/UNLIMITED ☒ SAME AS RPT ☒ DTIC USERS | Unclassified |
| 22a NAME OF RESPONSIBLE INDIVIDUAL | 22b TELEPHONE (Include Area Code) / 22c OFFICE SYMBOL |

DD FORM 1473, 84 MAR 83 APR edition may be used until exhausted
All other editions are obsolete

SECURITY CLASSIFICATION OF THIS PAGE
UNCLASSIFIED

TITLE: VIBRATION CONTROL IN ROTATING MACHINERY

USING VARIABLE DYNAMIC STIFFNESS SQUEEZE - FILMS.

VOLUME 2.

1st Full Interim Scientific Report Covering the period September 1984 - March 1986.

by

M J Goodwin

M P Roach

## 1. PROLOGUE

This report is a second volume of the 1st full interim scientific report (1) for the project described in the title, covering the period from month 1 to month 12 of the project. These programme months, which are indicated in figure 1 (which is an extract of figure 7 of the original grant proposal submitted to EOARD) correspond to calendar months March 1985 to March 1986. The programme of work did not begin in September 1984, as was originally intended, for a number of reasons; these are

(i) The grant funding was not submitted to the Polytechnic until October 1984.

(ii) The Polytechnic regulations forbid any attempt to advertise research assistant posts until the appropriate research funds are in the Polytechnic's hands.

(iii) There was a delay of 2 - 3 weeks between ordering an advert with newspaper publishers and the advert actually appearing in press.

(iv) The first round of advertising failed to result in the recruitment of a suitable applicant, so that a second round of advertising was necessary, causing a further delay of 2 - 3 weeks. The second round of adverts were ordered at about the end of November 1984 and appeared in January's press. (It was considered prudent not to publish an advert over the Christmas vacation period, so this also caused a further 2 weeks delay).

(v) The successful applicant was interviewed in February 1985 and commenced work in March 1985.

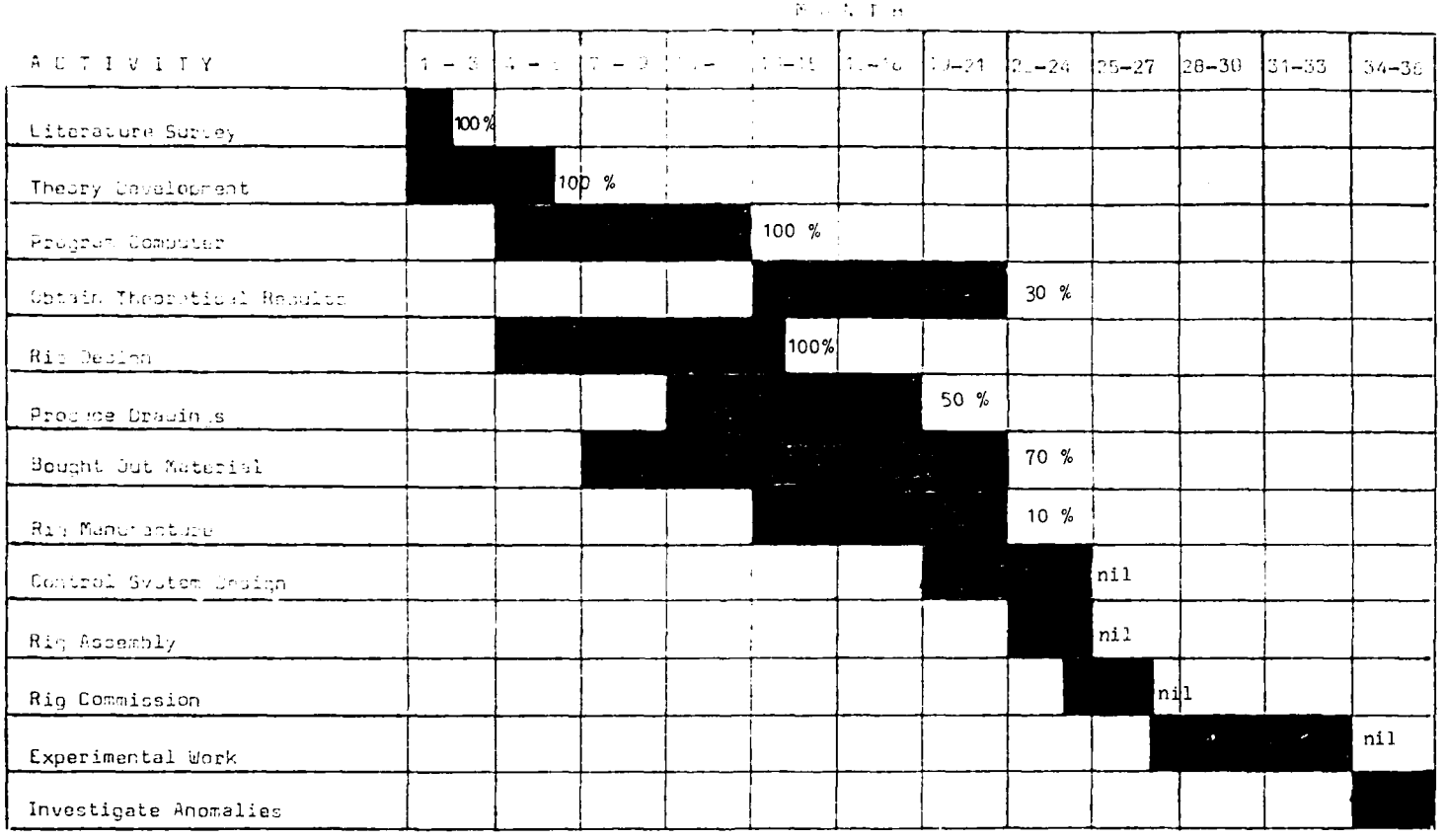


Figure 1: Programme of Research Project

As a consequence the above-described delay in the start of the project work, by August 1985 when the 1st volume of the 1st full interim scientific report was written, the work carried out to that moment in time corresponded to about 5 months work on the project schedule in figure 1. Thus, volume 1 of this report contains information relating mainly to a literature survey of hydrostatic bering operation, together with some details of the appropriate theory of operation under steady loads. It is noteworthy that the project was at that time on schedule, bearing in mind the programme start of March 1985.

The authors now understand that the delay in the start of the work had not been communicated to the American offices of EOARD (although it had been discussed with the London Office).As a consequence of the above situation the American offices of EOARD have requested further information about the project, particularly in relation to its current status and technical output. This second volume of the report is intended to answer fully any queries relating to the current status of the project, as well as to convey up to date technical information relating to the work.

## 2. INDEX OF CONTENTS

## 3. SYNOPSIS

This report describes the current status of a research project whose aim is to develop a hydrostatic bearing, for rotating machinery, whose dynamic characteristics may be tuned during operation of the machine. The purpose of this is to enable the operator to exercise some control over machine critical speeds, and vibrations generally.

A computer program has been written which will predict both the static and dynamic characteristics of a hydrostatic bearing. The program allows for the presence of accumulators linked to the hydrostatic bearing recesses via flow restrictors; by varying these flow restrictors control may be exercised over the bearing dynamic characteristics. Output from the computer program has been used as input data to a second computer program which calculates machine vibration amplitude variation with running speed. Theoretical machine characteristics obtained in this way have been used to aid the design of a test rig which will be used to examine the practical performance of the new bearing type being developed.

Theoretical results obtained thus far indicate that a significant change in bearing dynamic characteristics may be obtained by adjusting the accumulator flow restrictor, and that machine critical speeds can be reduced by over 50%. It appears likely that the bearing may enable maximum vibration amplitudes, within a given speed range, to be reduced by over 90%.

## 4. NOTATION

| SYMBOL | MEANING |
|---|---|
| A | Effective area of one hydrostatic pad |
| a | Cross-sectional area of capillary tube |
| B | Accumulator operating parameter |
| $C_{XX}$, $C_{XY}$; etc | Bearing damping coefficients |
| c | Bearing clearance |
| F | Force |
| I | Capillary restrictor inertia coefficient |
| K | Inverse flow resistance in capillary tube |
| $K_{XX}$, $K_{XY}$; etc | Bearing stiffness coefficients |
| L | Length of land around hydrostatic pad |
| l | Length of capillary tube |
| M | Mass of lubricant in capillary tube |
| P | Lubricant pressure |
| Q | Lubricant flow rate |
| R | Bearing radius |
| t | Time |
| V | Volume |
| v | Lubricant acceleration in capillary tube |
| W | Bearing land width |
| x | Horizontal displacement of journal |
| y | vertical displacement of journal |
| $\alpha$ | Half the included angle for one bearing pad |
| $\beta$ | Pressure $p_p/p_s$ at zero eccentricity |
| $\gamma$ | Pressure amplitude in accumulator |
| $\epsilon$ | Pressure amplitude in bearing pocket |
| $\xi$ | Phase lag angle of pressure amplitude in bearing pocket |
| $\theta$ | Angular location around bearing |
| $\kappa$ | Lubricant bulk modulus |
| $\mu$ | Lubricant dynamic viscosity |
| $\rho$ | Lubricant density |
| $\tau$ | Flow amplitude in supply line |
| $\psi$ | Flow amplitude in accumulator line |

| | |
|---|---|
| $\Phi$ | Phase lag angle of displacement in horizontal direciton |
| $\omega$ | Angular frequency |

SUBSCRIPTS

| | |
|---|---|
| a | Relates to accumulator |
| c | Relates to a curved land |
| l | Relates to flow over lands |
| nc | Relates to a non-curved land |
| p | Relates to bearing pocket |
| s | Relates to bearing supply line |
| v | Relates to change of pocket volume |
| x | Relates to horizontal direction |
| y | Relates to vertical direction |
| 1 | Relates to in-phase component |
| 2 | Relates to quadrature component |

## 5. INTRODUCTION

Unbalance in rotating machinery is responsible for vibration of the machine rotor, stator, and foundations. These vibrations result in high levels of noise, accelerated component wear, increased stresses and a lowering of the machines fatigue life. Unbalance cannot be completely eliminated but can only be minimised, and so these effects are always present; furthermore, some types of vibration are self-excited and are independent of the magnitude of the out of balance in the machine.

It is well documented, for example in references (1) to (5) that with all types of vibration the amplitudes of the rotor and bearing displacements, and of the bearing transmitted forces, are dependent upon the stiffness and damping associated with the bearings and their foundations. That is to say that for a given machine operating at a particular speed, the shaft support stiffness and damping must take on particular values in order to ensure that the system vibrations are mimimised. If these values are not adhered to then high levels of vibration will ensue.

In many cases the potentially large levels of vibration, dependent upon the shaft support stiffness and damping, are those associated with machine critical speeds. The designers problem is frequently one of ensuring that while a machine is able to operate at any particular speed within a given speed range, it must never be the case that a system critical speed is close to the operating speed. Unfortunately this is not easy to achieve because calculations of machine critical speeds are frequently inaccurate due to insufficient knowledge of bearing housing dynamic stiffness and of oil film behaviour. The situation is further complicated by the fact that bearing and foundation stiffness and damping in the horizontal sense may be different to that in the vertical sense, and so the number of machine critical speeds may be doubled.

The work to which this report relates is aimed at overcoming the problems described above by developing a bearing whose stiffness and damping could be altered while the machine is in operation. For example in figure 2 the solid line indicates the form of the response of a single mass rotor mounted on a shaft running in high stiffness supports.

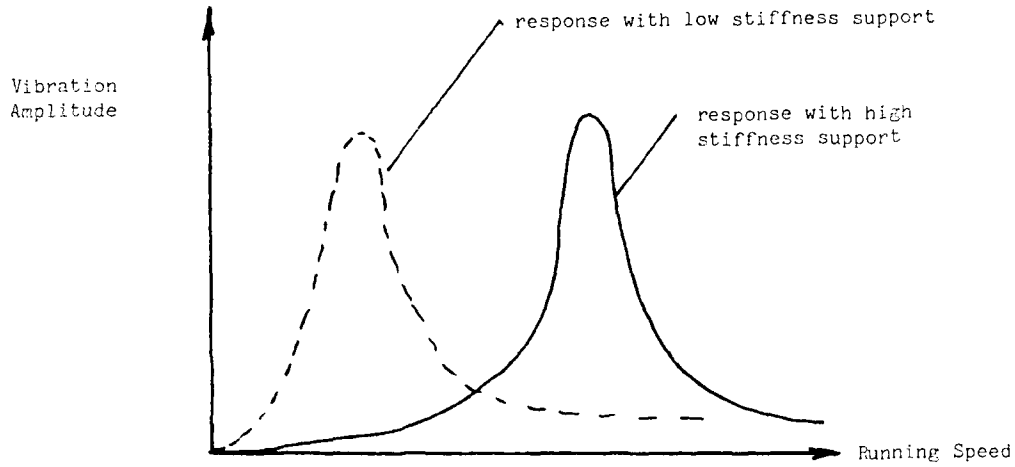


Figure 2: Typical Response of A Rotating Machine Operating Near its 1st Critical

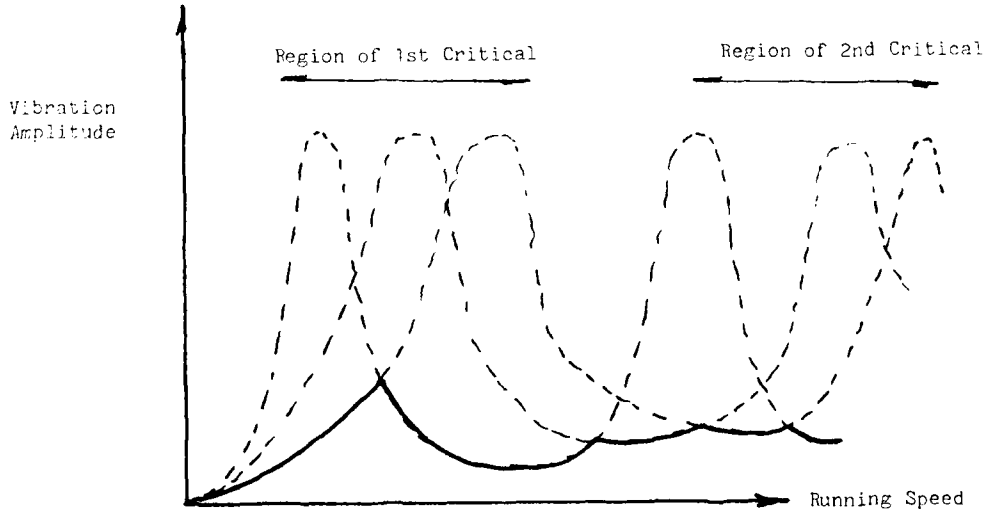


Figure 3: Vibration of a Multi-Degree of Freedom System

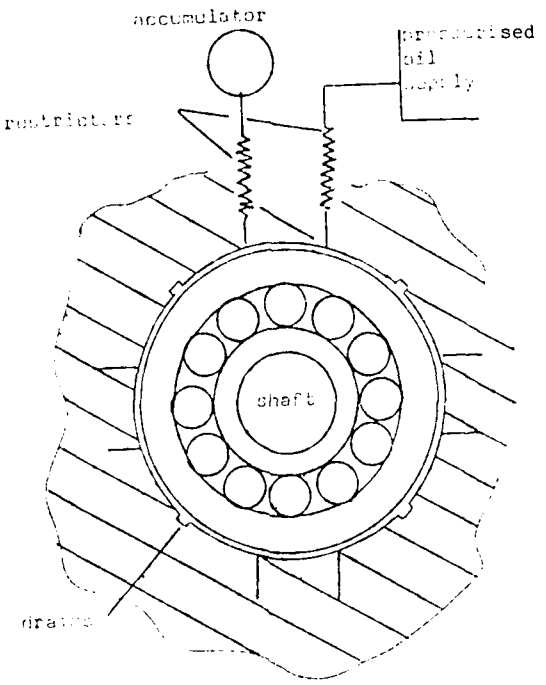


Figure 4: Arrangement of Bearing Type Investigated

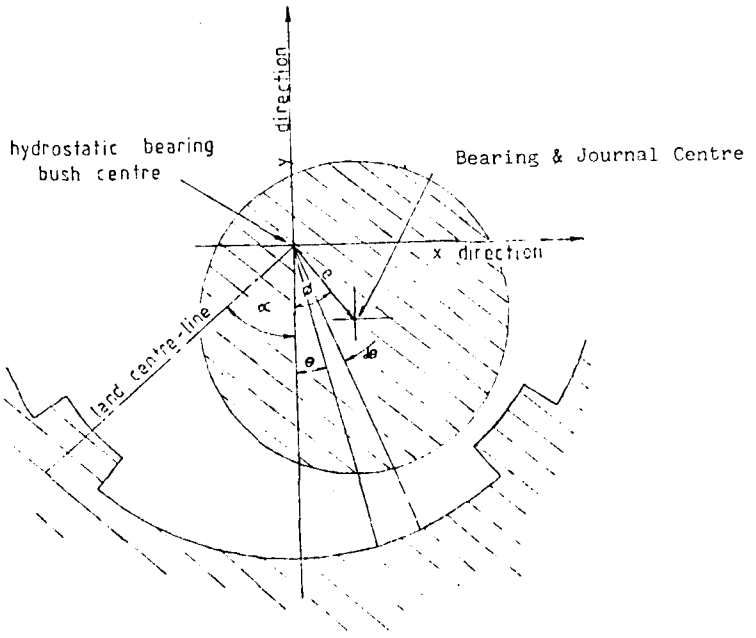


Figure 5: General View of One Hydrostatic Pad

The broken line represents the response of the same machine running in low stiffness supports. Clearly, as the machine speed was being increased, it would be advantageous to change the shaft support stiffness from a high value to a low value at the running speed corresponding to the point of intersection of the two curves. In the case of a multi-degree of freedom system it may be necessary to make use of several values of shaft support stiffness so that the machine response may be as indicated by the solid line in figure 3, the broken lines indicating critical speeds associated with particular values of shaft support stiffness.

This report describes an investigation of the effects of changing the shaft support stiffness and damping by building into the bearing supports a number of hydrostatic pads supplied with fluid under pressure via flow restrictors, the restrictors being required in order to ensure that the pads will support a static load in a stable manner. The case investigated was that of rolling element bearings, supported by hydrostatic pads as shown in figure 4. Also connected to the hydrostatic pads, via additional flow restrictors, are accumulators (closed vessels containing a gas-filled flexible bag, the gas, being relatively easy to compress, allows further oil to enter the accumulators in the space thereby made available). The accumulators behave as reservoirs from which oil may be drawn off or returned to. The stiffness and damping of such hydrostatic pads has been shown in references (6) and (7) to depend largely upon the flow resistance offered by the restictors in the accumulator lines. By varying the value of these flow resistances, the entire system support stiffness and damping can be varied between values close to zero and very high values.

## 6. THEORY

### 6.1 Review of Operation Under Steady Loads

Consider the hydrostatic bearing shown in figure 5 where the displacement of the (non-rotating) journal from the concentric position is $x_o$ in the horizontal direction and $y_o$ in the vertical direction. The concentric film clearance of the bearing under consideration is $C_o$, and if the journal eccentricity is e at an altitude angle $\Phi$ as shown, then the film clearance at any angle $\theta$ is

$$C = C_o - x_o \text{ Sin } \theta + y_o \text{ Cos } \theta \quad \ldots\ldots\ldots\ldots\ldots\ldots\ldots\ldots \quad (1)$$

A 'mid-land' type of approximation is now employed, similar to that used by Raimondi and Boyd (8). The approximation assumes that oil flows out over the bearing lands only in a direction perpendicular to the land centre-line, and that the pocket lubricant pressure effectively acts over an area contained within the land centre-lines. The accuracy of this approximation has been verified in reference (6).

If the bearing radius of curvature is R, the oil pressure in the pocket $P_p$, the oil dynamic viscosity $\mu$, hydrostatic pocket land width W, then the oil flow through an element $d\theta$ over one of the curved lands (not shown in figure 5) out of the plane of the page, is

$$dQ = \frac{C^3 \, R \, d\theta \, P_p}{12 \, \mu \, W} \quad \ldots\ldots\ldots\ldots\ldots\ldots\ldots\ldots\ldots\ldots \quad (2)$$

Substituting for C from equation (1) and integrating between $\theta = -\alpha$ and $\alpha$ gives the total oil flow out of the two curved lands of one hydrostatic pad as

$$Q_c = \frac{P_p \, R \, C_o^{\,3}}{12 \, \mu \, W} \left[4\alpha + \frac{1}{C_o} 12 \, \mu \text{ Sin } \alpha + \frac{1}{C_o^{\,2}}(6\alpha \, (y_o^{\,2} + x_o^{\,2}) + 3 \text{ Sin } 2\alpha \right.$$

$$\left. (y_o^{\,2} - x_o^{\,2})) + \frac{1}{C_o^{\,3}} \left(4y_o^{\,3} \left(\text{Sin } \alpha - \frac{\text{Sin}^3\alpha}{3}\right) + 12x_o^{\,2}y_o \, \frac{\text{Sin}^3\alpha}{3}\right) \right]. \quad \ldots \quad (3)$$

The total oil flow through the two non-curved lands at $\theta = \alpha$ and $\theta = -\alpha$ is

$$Q_{nc} = \frac{P_p L C_o^3}{12 \mu W} \left[(C_o + y_o \cos \alpha - x_o \sin \alpha)^3 \right.$$

$$\left. + (C_o + y_o \cos (-\alpha) - x_o \sin (-\alpha))^3\right] \quad \ldots\ldots\ldots\ldots\ldots\ldots (4)$$

which when expanded and added to equation (3) gives the total oil flow out of the bearing pocket over the lands as

$$Q_l \quad \frac{P_p C_o^3}{12 \mu W} \cdot f(x_o, y_o) \quad \ldots\ldots\ldots\ldots\ldots\ldots\ldots\ldots (5)$$

where

$$f(x_o, y_o) = (2L + 4R\alpha) + \frac{1}{C_o} (12Ry_o \sin \alpha + 6Ly_o \cos \alpha)$$

$$+ \frac{1}{C_o^2} (6R\alpha (y_o^2 + x_o^2) + 3R \sin 2\alpha (y_o^2 - x_o^2)$$

$$+ 6y_o^2 L \cos^2\alpha + 6x_o^2 L \sin^2\alpha)$$

$$+ \frac{1}{C_o^3} (4Ry_o^3 (\sin \alpha - \frac{\sin^3 \alpha}{3}) + 12Rx_o^2 y \frac{\sin^3 \alpha}{3}$$

$$+ 2Ly_o^3 \cos^3\alpha + 6Lx_o^2 y \sin^2\alpha \cos \alpha) \quad \ldots\ldots\ldots\ldots\ldots (6)$$

The flow into the hydrostatic pocket through the capillary from the pressurised supply is

$$Q_s = K_s (P_s - P_p) \quad \ldots\ldots\ldots\ldots\ldots\ldots\ldots\ldots (7)$$

Where $K_s$ is a constant which describes the capillary flow restrictor characteristics, and $P_s$ is the lubricant supply pressure. Equating equation (7) with equation (5) gives

$$K_s(P_s - P_p) = \frac{P_p C_o^3}{12 \mu W} \cdot f(x_o, y_o) \quad \ldots\ldots\ldots\ldots\ldots\ldots (8)$$

Defining $\beta$ as the ratio $P_p/P_s$ when the journal is concentric with the bearing ($x_o = y_o = 0$), equation (8) gives, on re-arranging,

$$K_s = \frac{\beta}{1 - \beta} \cdot \frac{C_o^3}{12 \mu W} (4R\alpha + 2L) \quad \ldots\ldots\ldots\ldots\ldots\ldots (9)$$

which defines the required value of $K_s$ to ensure that the bearing operates with a particular $\beta$ ratio. When this is the case, the pressure in the bearing pocket is then given by substituting equation (9) back into equation (8) to give

$$P_p = \frac{P_s \frac{\beta}{1 - \beta} (4R\alpha + 2L)}{\frac{\beta}{1 - \beta} (4R\alpha + 2L) + f(x_o, y_o)} \quad \ldots\ldots\ldots\ldots\ldots\ldots (10)$$

whereupon the steady load carried by the bearing may be evaluated as

$$F = Pp \cdot A \quad \ldots\ldots\ldots\ldots\ldots\ldots (11)$$

where $P_p$ is given by equation (10) and A is the bearing pad effective area contained within the land centre-lines.

The lubricant pumping power required by the bearing is given by

$$P = Qs \cdot P_s \quad \ldots\ldots\ldots\ldots\ldots\ldots (12)$$

The above-described theory was applied in turn to each hydrostatic pad of a 4 pad bearing (one hydrostatic pad at the top, bottom, and on each side of the bearing) and the corresponding forces separated out into vertical and horizontal components. The load components, oil flow, and pumping power for all of the hydrostatic pads may then be summed to give the characteristics of the whole bearing.

The above-described theory was transformed into a computer program to enable fast acquisition of design data to be made. The variation of load and static load stiffness with journal vertical displacements was found to take the form shown in figures 6 and 7 of section 6. These results are discussed in section 7.

## 6.2 Operation Under Dynamic Loads

When the bearing operates under the action of a dynamic load, the oil flow rate, pumping load, the oil flow rate, pumping power, and steady load supported remain unchanged. However, the bearing stiffness and damping become of prime importance because they affect substantially the vibration amplitude of the system for a particular force amplitude. A method of determining the bearing stiffness and damping is described below.

The displacement of the journal from the concentric position, under a dynamic load, takes the form

$$y = y_o + y_1 = y_o + Y \sin \omega t$$

$$x = x_o + x_1 = x_o + X \sin (\omega t - \Phi) \qquad \ldots\ldots\ldots\ldots\ldots\ldots (13)$$

where $x_1$ and $y_1$ are displacements of the journal from the static equilibrium position. As a consequence of these displacements the out flow of oil over the bearing lands of one hydrostatic pad differs from that given in equation (5) and is now given by

$$Q_1 \quad \frac{P_p C_o^3}{12 \mu W} \quad [f(x_o, y_o) + f_{xo}, x_1 + f_{yo}, y_1] \qquad \ldots\ldots\ldots\ldots (14)$$

where $f_{xo}$ and $f_{yo}$ are the differentials of $f(x_o, y_o)$ with respect to $x_o$ and $y_o$ respectively.

An alternative flow path for lubricant leaving the pocket is that through the flow restrictor leading to the accumulator. (This flow path is of no consequence when considering steady-state loads, since the accumulator forms a closed part of the system with a zero net flow into it). Any flow from the bearing pocket into the accumulator is as a consequence of a pressure difference between the lubricant in the bearing pocket and that in the accumulator. This pressure difference acts against the capillary flow resistance and also acts to accelerate the fluid in the capillary such that

$$P_p - P_a = \frac{1}{K_a} \cdot Q_a + I_a \cdot \frac{dQ_a}{dt} \quad \ldots\ldots\ldots\ldots\ldots\ldots\ldots\ldots (15)$$

where $P_a$ is the instantaneous lubricant pressure in the accumulator, $K_a$ is the constant describing the characteristics of the capillary flow restictor between the bearing and accumulator, $Q_a$ is the lubricant flow rate into the accumulator, and $I_a$ is a coefficient describing the inertia of the lubricant within the accumulator capillary.

The pressure changes within the accumulator are related to the volume of oil flowing into it by the equation

$$\frac{dP_a}{dt} = B\, Q_a \quad \ldots\ldots\ldots\ldots\ldots\ldots\ldots\ldots\ldots\ldots\ldots\ldots (16)$$

where B is a constant which describes the characteristics of the accumulator.

The flow of lubricant from the supply into the bearing pocket is described similarly by the equation

$$P_s - P_p = \frac{1}{K_s} \cdot Q_s + I_s \frac{dQ_s}{dt} \quad \ldots\ldots\ldots\ldots\ldots\ldots\ldots\ldots (17)$$

where $Q_s$ is the lubricant flow rate from the supply into the bearing pocket, and $l_s$ is a coefficient describing its inertia.

Any flow of oil into the bearing may be partially accomodated by an increase in the bearing volume, as the bearing surfaces move away from each other (and vice-versa). This flow may be represented, for a velocity dy/dt of the bearing surfaces away from each other, as

$$Q_v = A \frac{dy}{dt} \quad \ldots\ldots\ldots\ldots\ldots\ldots\ldots\ldots\ldots\ldots\ldots\ldots \quad (18)$$

In addition to the above, lubricant flowing into the bearing pocket may also be accomodated as a consequence of compressing the lubricant already in the clearance volume. The flow rate associated with compressibility of the lubricant is given by

$$Q_c = \frac{V_p}{K} \frac{dP_p}{dt} \quad \ldots\ldots\ldots\ldots\ldots\ldots\ldots\ldots\ldots\ldots\ldots\ldots \quad (19)$$

where $V_p$ is the bearing pad effective clearance volume and K is the lubricant bulk modulus.

The unsteady state flow equation for lubricant within the bearing pocket takes the form

$$Q_s = Q_a + Q_l + Q_v + Q_c \quad \ldots\ldots\ldots\ldots\ldots\ldots\ldots\ldots\ldots\ldots\ldots\ldots \quad (20)$$

The journal displacements, and the lubricant flow rates and pressures, may be assumed to vary according to the following expressions provided that amplitudes are small compared with steady-state values.

$$y = y_o + Y_1 \sin \omega t$$

$$x = x_o + X_1 \sin \omega t + X_2 \cos \omega t = x_o + X \sin (\omega t + \Phi)$$

$$P_p = P_{po} + \epsilon_1 \sin \omega t + \epsilon_2 \cos \omega t = P_{po} + \epsilon \sin (\omega t + \xi)$$

$$P_a = P_{po} + \gamma_1 \sin \omega t + \gamma_2 \cos \omega t$$

$$Q_s = Q_{so} + \tau_1 \sin \omega t + \tau_2 \cos \omega t$$

$$Q_a = Q_{ao} + \psi_1 \sin \omega t + \psi_2 \cos \omega t$$

In the above, the terms with suffices 1 and 2 are 'in-phase' and 'quadrature' values of the fluctuations in the displacement, pressure, and flow terms as appropriate.

Substituting equations (21) into equations (14) to (20), whilst also substituting equations (14), (18) and (19) into (20) gives:

$$\overset{*}{P}_{po} + (\epsilon_1 \sin \omega t + \epsilon_2 \cos \omega t) - \overset{*}{P}_{ao} - (\gamma_1 \sin \omega t + \gamma_2 \cos \omega t)$$

$$\frac{1}{K_a} (\overset{*}{Q}_{ao} + \psi_1 \sin \omega t + \psi_2 \cos \omega t) + I_a \omega (\psi_1 \cos \omega t - \psi_2 \sin \omega t) \quad . \quad (22)$$

$$\gamma_1 \omega \cos \omega t - \gamma_2 \omega \sin \omega t - B (Q_{ao} + \psi_1 \sin \omega t + \psi_2 \cos \omega t) \quad . \quad . \quad . \quad . \quad (23)$$

$$\overset{*}{P}_s - (\overset{*}{P}_{po} + \epsilon_1 \sin \omega t + \epsilon_2 \cos \omega t) = \frac{1}{K_s} (\overset{*}{Q}_{so} + \tau_1 \sin \omega t + \tau_2 \cos \omega t)$$

$$+ I_s W (\tau_1 \cos \omega t - \tau_2 \sin \omega t) \quad . \quad . \quad . \quad . \quad . \quad . \quad . \quad . \quad . \quad . \quad . \quad . \quad . \quad . \quad . \quad (24)$$

$$\overset{*}{Q}_{so} + \tau_1 \sin \omega t + \tau_2 \cos \omega t = \overset{*}{Q}_{ao} + \psi_1 \sin \omega t + \psi_2 \cos \omega t$$

$$+ \frac{C_o^3 f(x_o y_o)}{12 \mu W} (\overset{*}{P}_{po} + \epsilon_1 \sin \omega t + \epsilon_2 \cos \omega t)$$

$$+ \frac{P_{po} C_o^3}{12 \mu W} f_{xo} (X_1 \sin \omega t + X_2 \cos \omega t)$$

$$+ \frac{P_{po} C_o^3}{12 \mu W} f_{yo} Y_1 \sin \omega t + A_w Y_1 \cos \omega t$$

$$+ \frac{V_p}{K} W (\epsilon_1 \cos \omega t - \epsilon_2 \sin \omega t) \quad . \quad . \quad . \quad . \quad . \quad . \quad . \quad . \quad . \quad . \quad . \quad . \quad . \quad . \quad . \quad . \quad . \quad (25)$$

The terms marked * in the above equations may all be deleted since they are either zero terms or they relate to steady conditions and equate on each side of the equations. Comparing the coefficients of Sin $\omega t$ and Cos $\omega t$ on each side of what remains of the equations (22) to (25) then leads to the following equations which may be written in matrix form as:

$$\begin{bmatrix} 1 & 0 & -1/K_s & I_s\omega & 0 & 0 & 0 & 0 \\ 0 & -1 & -I_s\omega & -1/K_s & 0 & 0 & 0 & 0 \\ 1 & 0 & 0 & 0 & -1 & 0 & -1/K_a & I_a\omega \\ 0 & 1 & 0 & 0 & 0 & -1 & -I_a\omega & 1/K_a \\ 0 & 0 & 0 & 0 & 0 & -\omega & -B & 0 \\ 0 & 0 & 0 & 0 & \omega & 0 & 0 & -B \\ \frac{C_o^3 f(x_o\ y_o)}{12\ \mu\ W} & \frac{V_p\omega}{K} & 1 & 0 & 0 & 0 & 1 & 0 \\ \frac{V_p\omega}{K} & -\frac{C_o^3 f(x_o\ y_o)}{12\ \mu\ W} & 0 & 1 & 0 & 0 & 0 & -1 \end{bmatrix} \begin{bmatrix} \epsilon 1 \\ \epsilon_2 \\ \tau 1 \\ \tau_2 \\ \gamma_1 \\ \gamma_2 \\ \psi_1 \\ \psi_2 \end{bmatrix} =$$

$$\begin{bmatrix} 0 \\ 0 \\ 0 \\ 0 \\ 0 \\ 0 \\ \frac{C_o^3 P_{po} (f_{xo} X_1 + f_{yo} Y_1)}{12\ \mu\ W} \\ \frac{C_o^3 P_{po} f_{xo} X_2 + A\omega Y_1}{12\ \mu\ W} \end{bmatrix} \quad \ldots\ldots\ldots\ldots\ldots\ldots (26)$$

The inertia terms $I_s$ and $I_a$ in the above equation may be determined by applying Newtons 2nd law to the column of liquid contained within the capillary.

Thus

$$\Delta P . a = m \dot{v} \quad \ldots\ldots\ldots\ldots\ldots\ldots\ldots\ldots\ldots\ldots\ldots\ldots (27)$$

where $\Delta P$ is the pressure difference across the capillary, a is the bore cross-sectional area, m the mass of lubricant within the capillary, and $\dot{v}$ its acceleration. Equation (27) may also be written as

$$\Delta P = \frac{m}{a} \dot{v}$$

$$\frac{l \rho \dot{Q}}{a} \quad \ldots\ldots\ldots\ldots\ldots\ldots\ldots\ldots\ldots\ldots\ldots\ldots (28)$$

where l is the length of the capillary tube, $\rho$ is the lubricant density, and Q is the flow rate through the capillary. Further consideration of equations (15) and (17) reveals that the capillary inertia coefficient is then given by

$$I = \frac{l \rho}{a} \quad \ldots\ldots\ldots\ldots\ldots\ldots\ldots\ldots\ldots\ldots\ldots\ldots (29)$$

Equation (26) may be solved to determine the unknown amplitudes of the variables in the column matrix on the left hand side, in particular the pocket pressure amplitudes $\epsilon_1$ and $\epsilon_2$.

The force-displacement relationship for one hydrostatic pad under dynamic operating conditions takes the form

$$F_y = K_{yy} y_1 + K_{yx} x_1 + C_{yy} \dot{y}_1 + C_{yx} \dot{x}_1 \quad \ldots\ldots\ldots\ldots\ldots\ldots (30)$$

where $K_{yy}$, $K_{yx}$, $C_{yy}$ and $C_{yx}$ are the direct and cross-coupling stiffness and damping coefficients for one bearing pad. $F_y$ is the load on the pad (in the vertical direction); the arrangement may be considered to be as shown in figure 3. The variation in force $F_y$ on the pad will be related to the bearing pocket oil pressure by

$$F_y = A (\epsilon_1 \text{ Sin } \omega t + \epsilon_2 \text{ Cos } \omega t) \quad \ldots\ldots\ldots\ldots\ldots\ldots (31)$$

Substituting for x and y from equations (21) and for $F_y$ from (31) into equation (30), and comparing coefficients of sin $\omega t$ and Cos $\omega t$ gives

$$A\epsilon_1 = K_{yy} Y_1 + K_{yx} X_1 - \omega C_y X_2$$

$$A\epsilon_2 = K_{yx} X_2 + \omega C_{yy} Y_1 + \omega C_{yx} X_1 \quad \ldots\ldots\ldots\ldots\ldots\ldots (32)$$

If we then set $X_1 = X_2 = 0$, then

$$K_{yy} = \frac{A\epsilon_1}{Y_1}$$

$$C_{yy} = \frac{A\epsilon_2}{\omega Y_1} \quad \ldots\ldots\ldots\ldots\ldots\ldots\ldots\ldots (33)$$

whilst if we set $Y_1 = X_2 = 0$, then

$$K_{yx} = \frac{A\epsilon_1}{X_1}$$

$$C_{yx} = \frac{A\epsilon_2}{\omega X_1} \quad \ldots\ldots\ldots\ldots\ldots\ldots\ldots\ldots (34)$$

Thus all four linearized stiffness and damping coefficients for one hydrostatic pad are determined.

The above theory was transformed into a computer program enabling stiffness and damping coefficients for each hydrostatic pad in the bearing to be computed, in terms of its local coordinates. These coefficient values were then transformed into corresponding values of the global coordinates as described in reference (6) and summed to determine net coefficient values for the whole bearing. The program was used to investigate the variation in bearing stiffness and damping with journal eccentricity, capillary inertia coefficient, accumulator restrictor coefficient, and forcing frequency. The results of this investigation are also summarized in the section 6.

### 6.3 Rotor Response

The bearing stiffness and damping coefficient values determined as described in the previous section were used as input data to a third computer program which has been used previously by the authors to determine rotor response. This program is based on the transfer matrix method. The method is well-known by rotordynamicst and so will not be described in detail in this report for the sake of brevity; further details of the method may be found in references (9) to (11).

The system design parameters used in this investigation were similar to those of a real aeroengine compressor shaft system. It was decided that a rotor whose mass was mainly located at midspan be investigated, since it was intended that the experimental test rig rotor would feature this characteristic, for the sake of simplicity. The other details of the system were as shown in table 1. A description of the system modelled is given in section 9. The following section shows the results of the investigation, indicating the variation in rotor vibration amplitude with running speed for two values of accumulator restrictor setting.

| | |
|---|---|
| Bearing Details:- | |
| Hydrostatic pad arrangement: | 1 at each of top, bottom, and sides; ie 4 total per bearing |
| Lubricant supply pressure: | 2.5 Mpa |
| Compensation: | Capillary tube |
| Nominal radial clearance: | 127 μm |
| Land width: | 5 mm |
| Bearing diameter: | 0.1 m |
| Bearing length: | 0.025 m |
| Lubricant viscosity: | 0.05 Pa.s |
| Design pressure ratio, $\beta$: | 0.5 |
| Lubricant bulk modulus: | 1.7 GPa |
| Recess Depth: | 10 mm |
| Rotor Details: | |
| Length between bearings: | 0.5 m |
| Shaft diameter: | 0.04 m |
| Shaft bending stiffness: | 9.6 MNm $^{-1}$ |
| Rotor mass: | 35 Kg |
| Rotor diameter: | 0.4 m |
| Rotor length: | 0.08 m |
| Nominal maximum speed: | about 10,000 rev/min |
| Operating range of shaft/bearing stiffness ratio: 0.1 - 6.0 | |

Table 1: Details of Machine Design used for the Theoretical Investigation.

## 7. RESULTS

This section contains the results of the theoretical investigation of the hydrostatic bearing static and dynamic characteristics, and of the vibration amplitude variation with running speed of a single mass rotor running in such bearings. The results relate to a machine whose design features are similar to those indicated in table 1, unless stated otherwise.

The following results are included in this section:

Figure 6 Variation of bearing load with journal eccentricity

Figure 7 Variation of steady load stiffness with journal eccentricity

Figure 8 Variation of Bearing Stiffness coefficient $K_{yy}$ with vertical eccentricity

Figure 9 Variation of Bearing Damping coefficient $C_{yy}$ with vertical eccentricity

Figure 10 Variation of Bearing Stiffness coefficient $K_{yy}$ with horizontal eccentricity

Figure 11 Variation of Bearing Damping coefficient $C_{yy}$ with horizontal eccentricity

Figure 12 Variation of Bearing Stiffness coefficient $K_{xy}$ with vertical eccentricity

Figure 13 Variation of Bearing Damping coefficient $C_{xy}$ with vertical eccentricity

Figure 14 Variation of Bearing Stiffness coefficient $K_{yx}$ with vertical eccentricity

Figure 15 Variation of Bearing Damping coefficient $C_{yx}$ with vertical eccentricity

Figure 16 Variation of Bearing Stiffness coefficient $K_{yy}$ with frequency

Figure 17 Variation of Bearing Damping coefficient $C_{yy}$ with frequency

Figure 18 Variation of Bearing Stiffness coefficient $K_{yy}$ with Accumulator Restrictor

Figure 19 Variation of Bearing Damping coefficient $C_{yy}$ with Accumulator Restrictor

Figure 20 Variation of Rotor 1st critical speed with support stiffness

Figure 21 Variation of Rotor Vibration amplitude with running speed

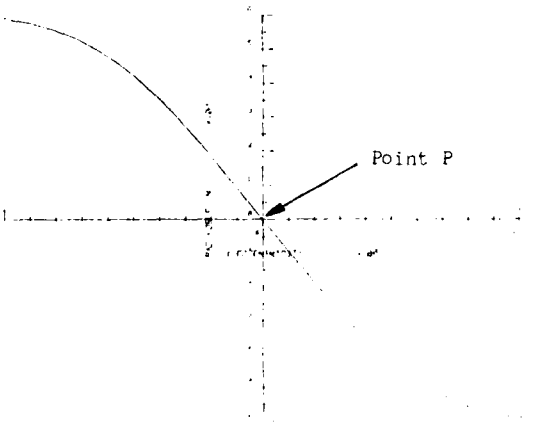


Figure 6: Variation of Bearing Force with Eccentricity
$\beta = 0.5$

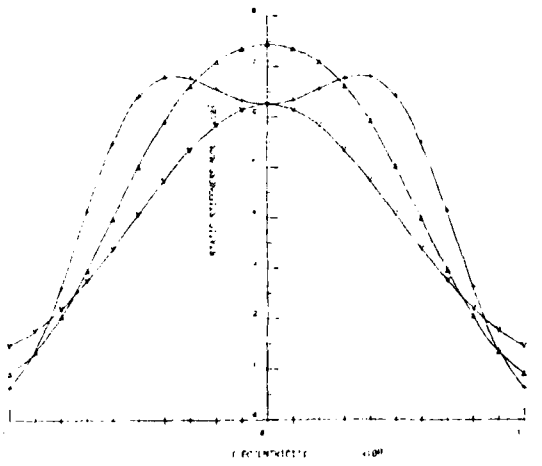


Figure 7: Variation of Steady Load Stifness with Eccentricity
$\beta = 0.5$

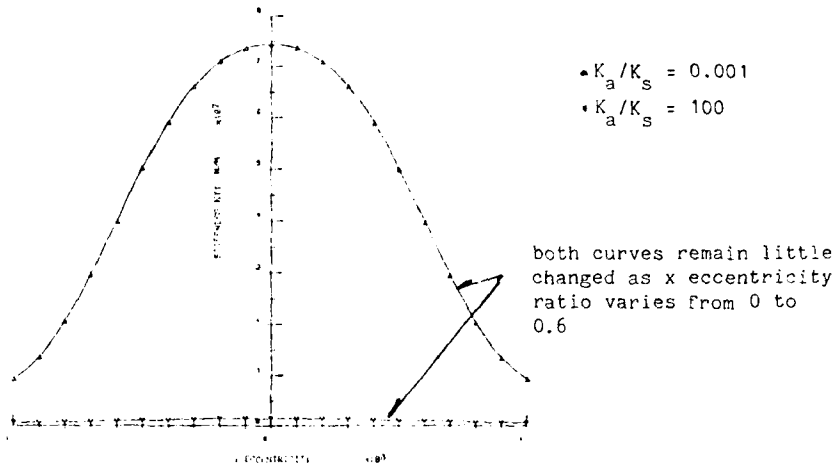


Figure 8: Variation of Bearing Stiffness Coefficient $K_{yy}$ with Vertical Eccentricity

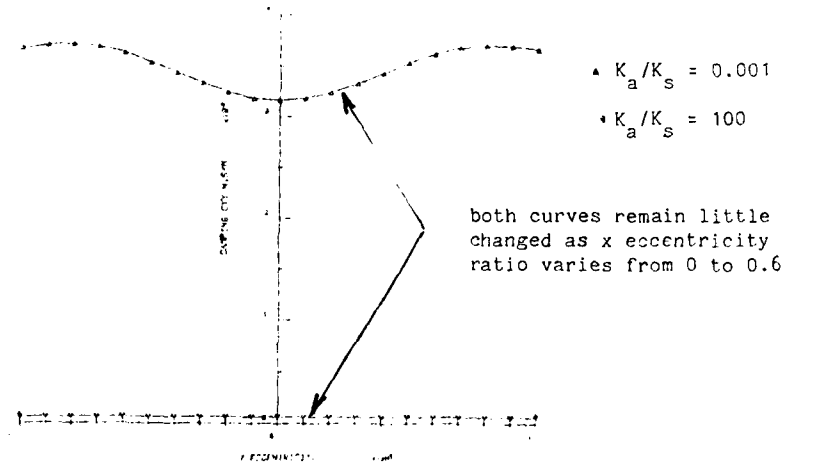


Figure 9: Variation of Bearing Damping Coeficient $C_{yy}$ with Vertical Eccentricity

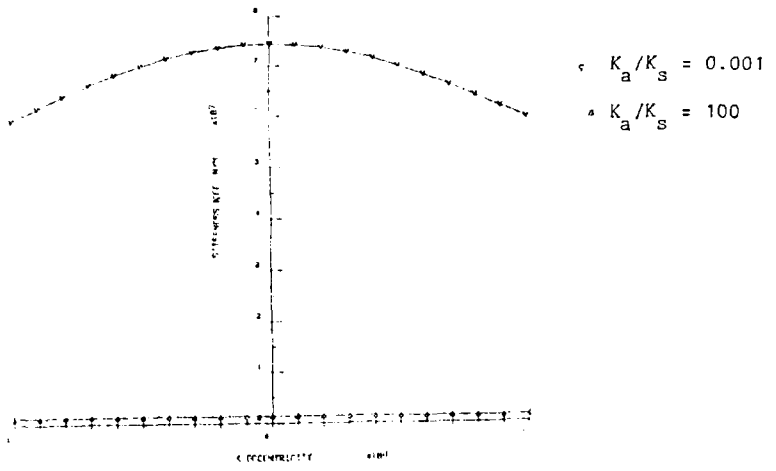


Figure 10: Variation of Bearing Stiffness Coefficient $K_{yy}$ with horizontal eccentricity

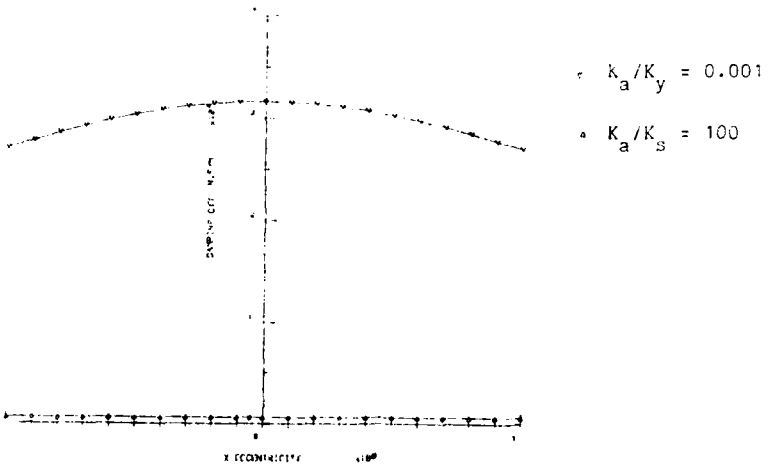


Figure 11: Variation of Bearing Damping Coefficient $C_{yy}$ with horizontal eccentricity

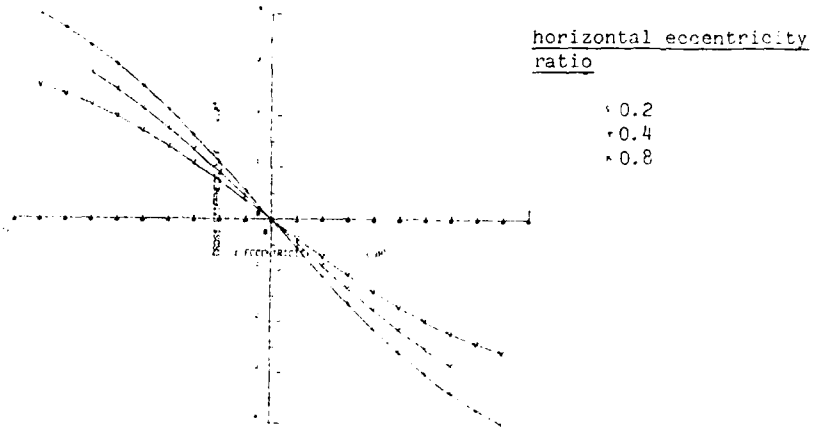


Figure 12: Variation of Bearing Stiffness Coefficient $K_{xy}$ with vertical eccentricity

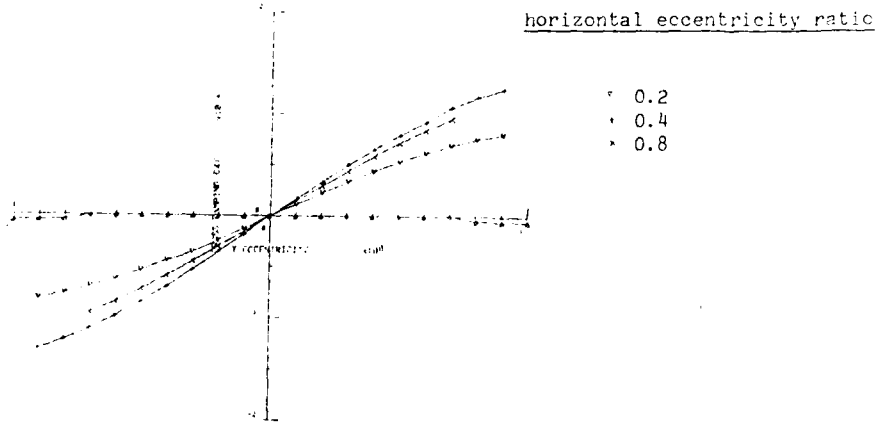


Figure 13: Variation of Bearing Damping Coefficient $C_{xy}$ with vertical eccentricity

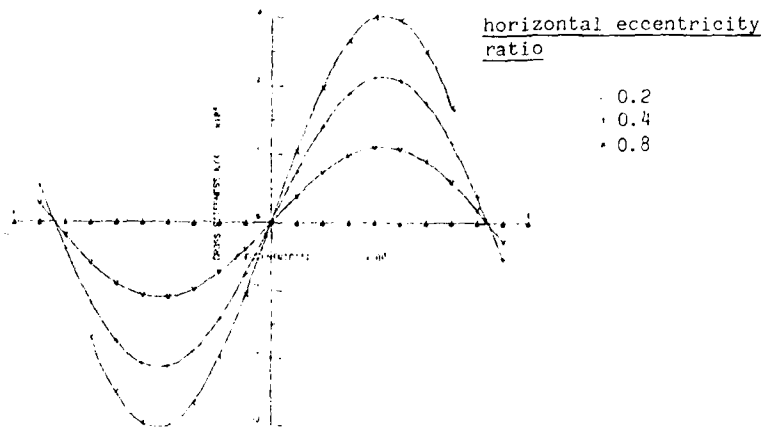


Figure 14: Variation of Bearing Stiffness Coefficient $K_{yx}$ with vertical eccentricity

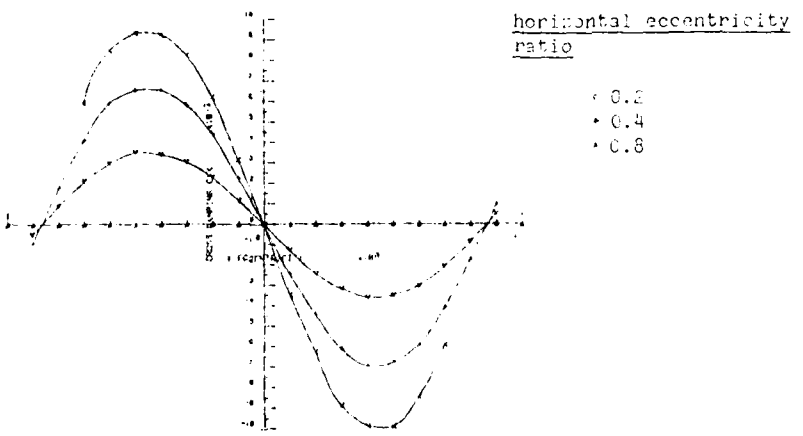


Figure 15: Variation of Bearing Damping Coefficient $C_{yx}$ with vertical eccentricity

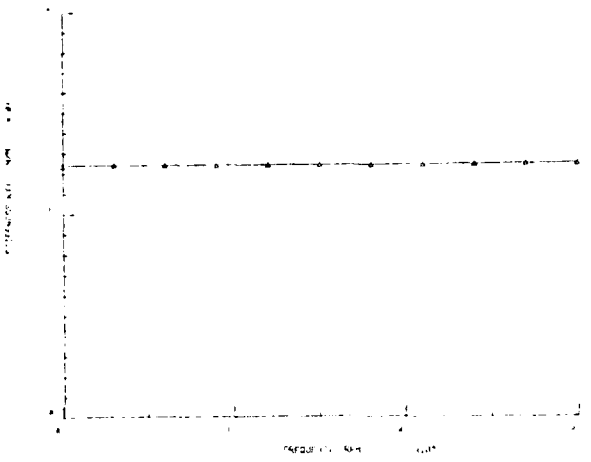

Figure 16: Variation of Bearing Stiffness Coefficient $K_{yy}$ with Frequency

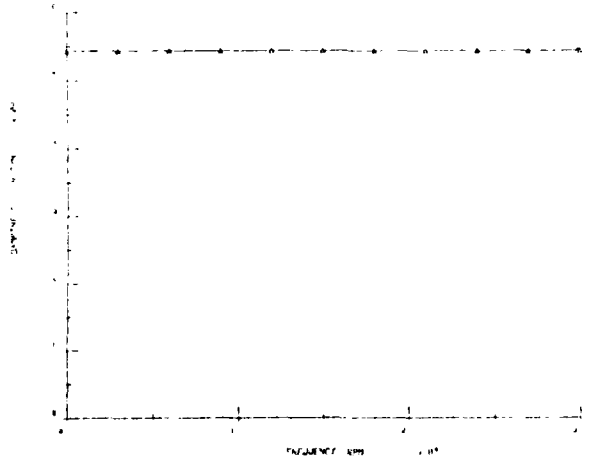

Figure 17: Variation of Bearing Damping Coefficient $C_{yy}$ with Frequency

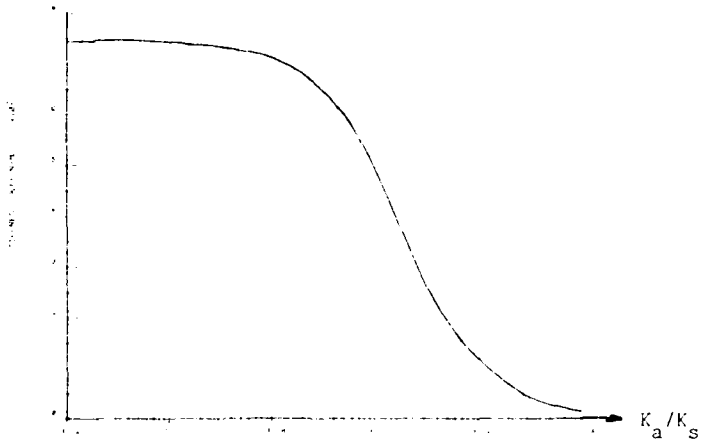


Figure 18: Variation of Bearing Stifnes Coefficient $K_{yy}$ with Ratio of Supply/Accumulator Flow Resistance

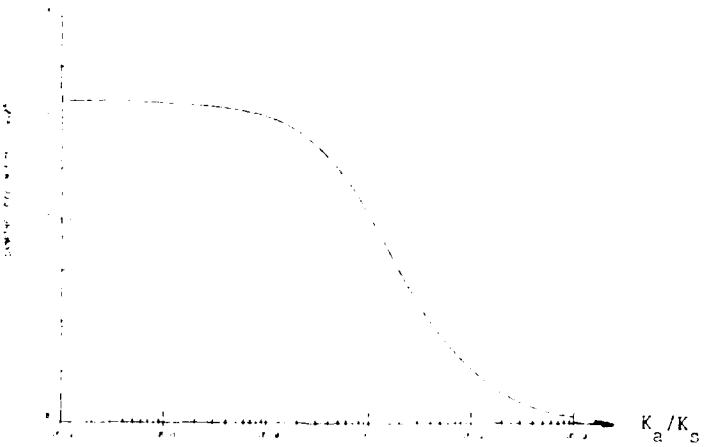


Figure 19: Variation of Bearing Damping Coefficient $C_{yy}$ with Ratio of Supply/Accumulator Flow Resistance

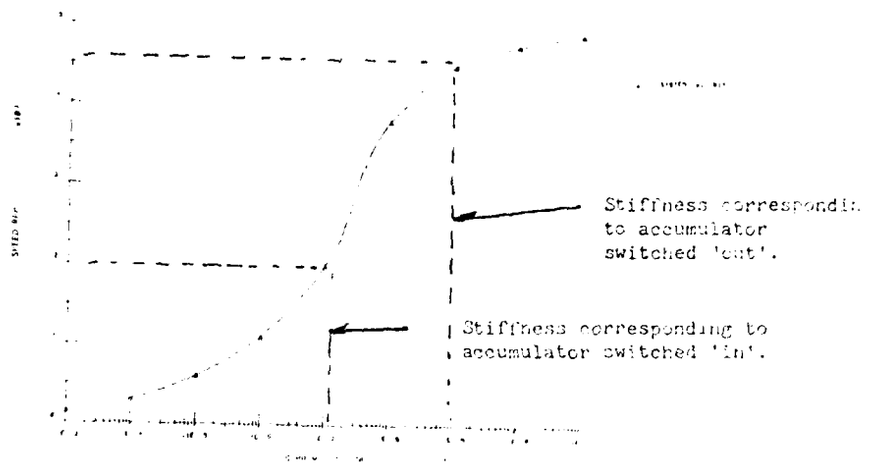


Figure 20: Variation of Rotor 1st Critical Speed with Support Stiffness

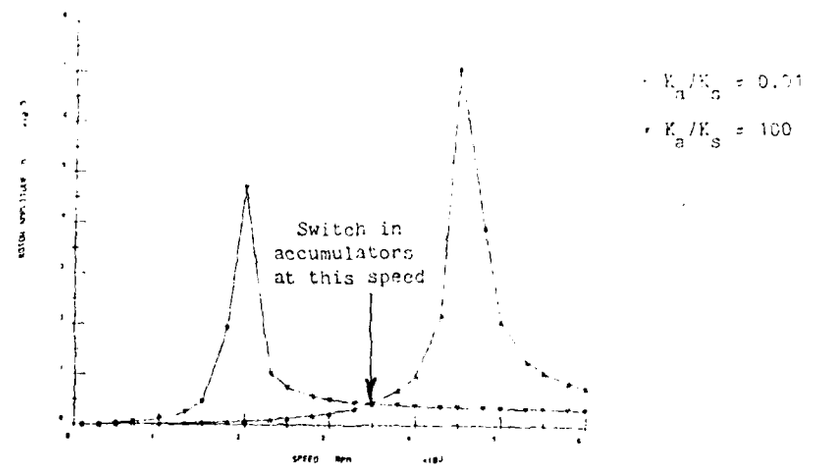


Figure 21: Theoretical Response of Rotor

## 8. DISCUSSION

Figure 6 shows the variation in steady vertical displacement with static vertical load for the hydrostatic bearing. As is normally the case with hydrostatic bearings, the authors have decided to operate with a pressure ratio $\beta = 0.5$ at the nominal design clearance since this will result in an oil film of higher stiffness (so far as operation under static loading is concerned). The gravity load on each bearing is calculated to be about 200 N, so that each hydrostatic bearing will operate at an eccentricity ratio of approximately zero see point P on figure 6.

The variation of steady load stiffness with vertical eccentricity is shown in Figure 7. Stiffness decreases with increasing bearing eccentricity in general, irrespective of the bearing pressure ratio $\beta$. For this reason the design pressure ratio is chosen on the basis of maximum stiffness at the design eccentricity only.

Figure 8 shows the variation in hydrostatic bearing stiffness coefficient $K_{yy}$ with vertical displacement for various horizontal displacements. It is noteworthy that its value does not change significantly with horizontal displacement, although it does with vertical displacement. Under normal operating conditions the bearing will be operating at a virtually zero vertical eccentricity (as well as zero horizontal eccentricity) so that the stiffness coefficient $K_{yy}$ will assume a maximum value. Despite the non linearity of the curve, it can be seen from the effective oil film coefficient value would not be expected to change by more than 10% of its original value provided that the vibration amplitude does not exceed 0.2 times the nominal bearing clearance.

Figure 9 shows the variation in hydrostatic bearing damping coefficient $C_{yy}$ with vertical displacement for various horizontal displacements. In this case the coefficient value does not change significantly with either horizontal or vertical displacement. This means that the value of damping coefficient $C_{yy}$ can be calculated accurately at the design stage and that non linearity of this coefficient is unlikely to present a problem.

Figures 10 and 11 show the variation of horizontal stiffness and damping coefficients $K_{yy}$ and $C_{yy}$ respectively with horizontal eccentricity. These coefficients do not change significantly with horizontal eccentricity, and so once again coefficient non linearity is unlikely to present a problem. Once again, the coefficients take a maximum value when the bearing operates in the concentric position.

The Variation of bearing horizontal stiffness and damping coefficients $K_{xx}$ and $C_{xx}$ with horizontal and vertical eccentricity is identical to that of coefficients $K_{yy}$ and $C_{yy}$ with vertical and horizontal eccentricity respectively. For the sake of brevity the corresponding curves have not been included in this report.

Figure 12 to 15 show the variation of the cross coupling stiffness and damping coefficients $K_{xy}$, $K_{yx}$, $C_{xy}$ and $C_{yx}$ with displacement. These coefficient values are all much smaller than the values of the direct terms discussed above and so are of little significance; in any instance they all assume a zero value when the bearing operates at zero eccentricity as will be the case for the test rig with which this project is concerned. These graphs are included in this report only for the sake of completeness of records.

Figures 16 and 17 show the variation in stiffness and damping coefficient, $K_{yy}$ and $C_{yy}$ respectively, with excitation frequency. For the frequency range under investigation it is clear that the coefficient values do not change significantly. This feature of the results is significant since it indicates that the inertia of the lubricant within the capillary restrictors is unlikely to affect the behaviour of the bearing adversely. The other six bearing coefficients are similarly unaffected by frequency of excitation; the appropriate curves for these coefficients have been omitted from this report for the sake of brevity.

The variation in bearing stiffness and damping with flow resistance between bearing recess and accumulator is shown in figures 18 and 19. (These graphs relate to coefficients $K_{yy}$ and $C_{yy}$; once more graphs for the other coefficients have been omitted for the sake of brevity but do in fact take on similar features).

It can be seen that when the flow resistance into the accumulator is large ie when $K_a/K_s$ is small then the coefficients take on high values, whereas when the flow resistance is very small ($K_a/K_s$ large) the magnitude of the coefficients is reduced to about 5% of their original value. Thus, a substantial change in bearing dynamic coefficient values can be introduced by connecting an accumulator to the hydrostatic bearing recesses via a connector whose flow resistance is negligible.

This condition can be achieved in practice, if only two values of each bearing dynamic coefficient are required during operation, by connecting the accumulators to the bearing recesses via remotely-controlled on off valves with large bore diameters.

The variation in first critical speed with support stiffness for the test rig being constructed is shown in figure 20. The hydrostatic bearing has been designed so that the two values of bearing stiffness coefficients obtained with the accumulator switched 'in' and 'out' tend to straddle the steepest part of the graph as shown. It appears that with this arrangement the test rig first critical speed may be switched from about 4,600 rev/min to about 3000 rev/min. The corresponding response curves for the machine are shown in figure 21. In this figure it can be seen that if the accumulators are switched 'in' at about 3,500 rev/min, then the maximum amplitude of vibration of the machine during run up through the first critical speed region may be reduced from about 72 $\mu$m to about 7 $\mu$m for the example shown.

The form of each of the graphs discussed above was of direct relevance to the design of the test rig. In addition to these, a number of additional parameter relationships for the hydrostatic bearing have also been investigated. The appropriate results have been taken into account during the test rig design, but the form of the graphs is not of such direct significance and so they have been included in this report only as an appendix containing figures 23 to 30. These results may be summarised as follows:

a) Decreasing pressure ratio $\beta$ tends to increase bearing stiffness and damping, although stiffness actually 'peaks' at $\beta$ =0.5 in the case of a high flow resistance in the accumulator line (figures 23 and 24).

b) Increasing bearing clearance tends to reduce both the bearing damping and stiffness (figures 25 and 26).

c) Raising the lubricant supply pressure has little effect on the bearing damping, but does result in a proportional increase in bearing stiffness (figures 27 and 28).

d) Increasing the bearing land width has little effect on the bearing stiffness but does increase bearing damping (figures 29 and 30).

It is noteworthy that these relationships are in general agreement with those found in other literature relating to hydrostatic bearing performance. They are of interest because they provide additional information about how the bearing characteristics may be deliberately set at the design stage, once the required values have been determined.

To summarise, the hydrostatic bearing may be designed to accomodate the static load, due to rotor gravity forces, without significant eccentricity of the journal. The bearing dynamic characteristics of most significance are the direct stiffness and damping coefficients since the cross coupling coefficients are several orders of magnitude smaller. The direct stiffness and damping coefficients can be substantially reduced by connecting an accumulator to the bearing recess and, provided that the hydrostatic bearing is correctly designed for the rotor system under consideration, the stiffness change introduced can be made to result in a significant change in machine natural frequency. If the accumulator is switched 'in' at the correct rotational speed then the maximum vibration amplitude of the machine during run up may be reduced by over 90%. The required hydrostatic bearing dynamic characteristics can be obtained by correctly selecting appropriate design parameters for the bearing.

## 9. TEST RIG DESIGN

A test rig has been designed which will enable experimental evaluation of the new bearing design under consideration. The final details of the design have been established with a view to modelling the high speed compressor shaft of a General Electric TF34 turbofan engine, some details of which are given in reference (12). The only departure of the similarity of the experimental rig from that detailed in reference (12) is the absence of an overhung rotor mass in addition to that mounted between bearings. The test rig is designed to operate up to speeds well above its first critical speed of 5000 rev/min. A comparison of some of the design parameters of the TF34 turbofan engine with those of the test rig is shown in table 2. Some additional design details of the bearings to be used with the test rig are as used for the theoretical investigation, and are shown in table 1.

A diagram of the assembled test rig is shown in figure 22. It consists of a rotor of mass 35 kg mounted on a shaft of length 0.5 m. The shaft, whose stiffness is 9.6 $MN/m^{-1}$, runs in rolling element bearings which are pressed into a steel bush; the bush is in turn mounted in the hydrostatic bearings and is constrained not to rotate by anti rotation pegs. Each hydrostatic bearing contains four hydrostatic pads, as shown in figure 2b. The bearing operates with a concentric pressure ratio $\beta$ 0.5 to provide maximum resistance to journal displacement under gravity loads, the steady state journal eccentricity being negligible. Each bearing is supplied with lubricant of dynamic viscosity 0.05 Pas at a pressure of 2.5 M Pa. The hydrostatic bearing pedestals are mounted firmly on a fabricated bed-plate which is in turn fixed securely to the ground. The rig is powered by a variable speed electric motor which is remotely controlled.

Vibration measurements are recorded by non contracting inductive proximity transducers situated at each bearing and at the rotor mass. The output signals from the transducers are to be recorded by a microcomputer-controlled data-logging system which may also be used to help to process and plot the results.

| Property | Value on Test Rig | Value on TF34 Engine |
|---|---|---|
| Shaft Stiffness | 9.6 $MN/m^{-1}$ | 51 $MN/m^{-1}$ |
| Rotor Mass | 35 Kg | 40 Kg |
| 1st Critical Speed | 2500 - 5000 rev/min | 5000 rev/min |
| Ratio Shaft/Support Stiffness | 0.1 - 6.0 | normally between 0.6 and 2.5 |
| Running Speed | up to 10,000 rev/min | up to 17,600 rev/min |
| Lubricant Viscosity | 0.05 Pa.s | 0.04 Pa.s |

Table 2: A Comparison of some test rig details with those of a General Electric TF34 Turbofan Engine high speed shaft.

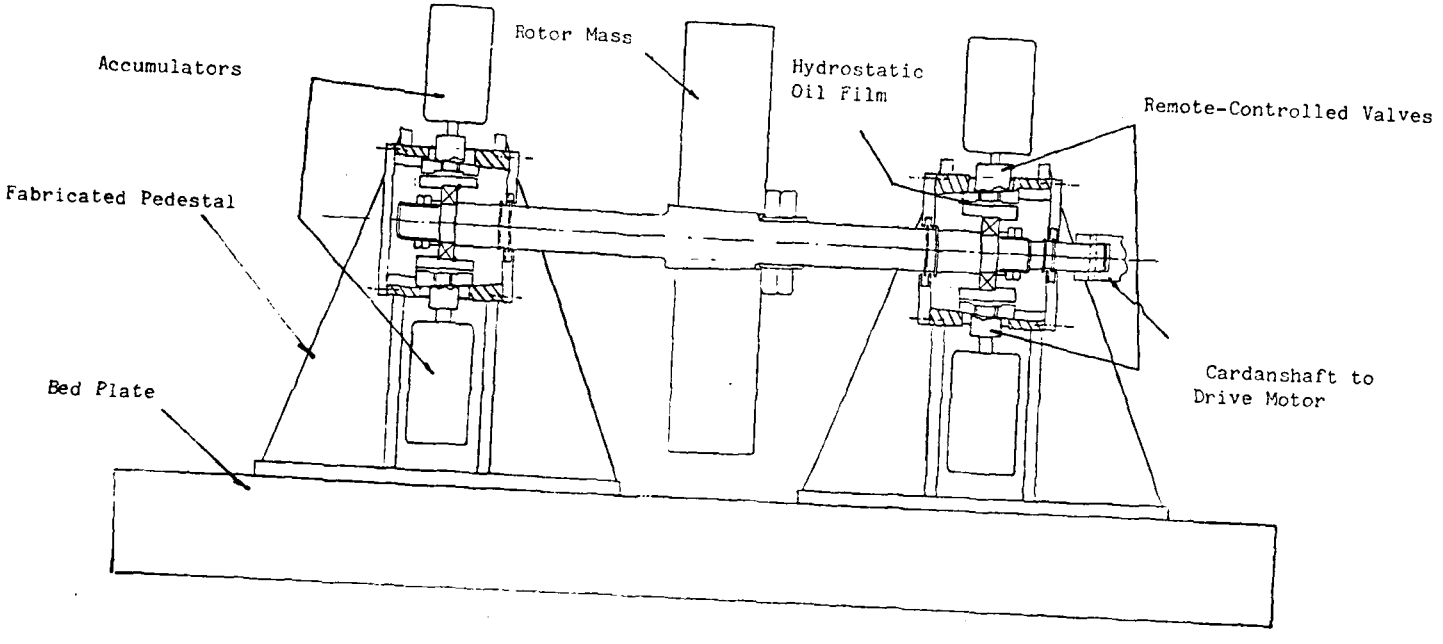


Figure 22: Diagram of Test Rig

## 10. REVIEW OF CURRENT STATUS OF PROJECT

The current status of the research project described in this report is indicated by figure 1. As explained in section 1 of this report, work began on the project in March 1985, as indicated in the figure, so that March 1986 corresponds to month 13.

For each activity indentified in figure 1, the percentage figure indicated on the appropriate line gives the fraction of that activity which has been completed at the time of writing this report. Those activities not yet completed are as follows:

(i) Obtain Theoretical Results

Some theoretical results are presented in this report; however the computer programs are to be re-run in order to further investigate the effect of system parameter changes, and the results are to be re-presented in dimensionless form.

(ii) Produce Drawings

Most of the engineering drawings required for test rig manufacture have been produced. It is possible that further auxilliary drawings detailing such items as balance ωts, wiring diagrams, lubrication systems, etc may be required.

(iii) Bought Out Material & Rig Manufacture

Test rig manufacture is about to commence. Most of the material required for this is in stock. Some further components such as piping, valves, and accumulators still need to be purchased. It is anticipated that the rig will be assembled by September 1986.

The authors overall opinion of the project status, bearing in mind the details indicated in figure 1, is that the project may be completed in slightly less time than the 36 months originally estimated. However, in so far as the original grant document is concerned, which was based on a project start date of September 1984, the authors anticipate possibly requiring an extension of the grant period at no extra cost.

## 11. CONCLUSIONS

It is clear from the results of several previous investigations discussed in section 5, and from the theoretical studies described in this report that machine vibration amplitudes can be minimized by correct choice of shaft support dynamic charateristics. It is further evident that changes in shaft support dynamic characteristics can substantially change machine critical speeds.

The theoretical studies described in this report have shown that hydrostatic bearing dynamic characteristics can be tuned by controlling flow restrictors which link accumulators to the bearing pockets. Furthermore, the changes in bearing stiffness and damping so implemented can be used to change significantly machine critical speeds. If the change in support stiffness is made while the machine is running then the maximum vibration amplitude during run up may be reduced, using this technique, by up to 90%.

The project status may be summarised as follows. The theory development and computer programming are virtually complete. The test rig design has been completed and manufacture is under way. During the coming months, while the rig is being manufactured, further theoretical results will be obtained from the computer output and consideration will be given to the test rig control system. The delay fo 6 months in commencing work on the project has, to a large extent, been recovered.

## 12. RECOMMENDATIONS FOR FURTHER WORK

Funding of the project has been provided by EOARD for two years to date, and this has either been expended or allocated according to the original research schedule plan contained in the grant proposal document (similar to figure 1 of this report). Some return on this investment has been obtained in the form of theoretical results contained within this report, and further theoretical results will be available shortly.

Further work should centre around obtaining experimental evidence to substantiate the theoretical results in order that the theory may be used with more confidence when applied to real aero-engine systems. The experimental testing should proceed according to the schedule in figure 1 using, (in the first instance), the test rig described in section 9. The experimental work should include measurements of machine vibration amplitude and frequency through the entire running speed range, this data should be collected for several values of accumulator restrictor setting, bearing oil supply pressure, and other pertinent parameters. Additional experimental test runs should be made using a microprocessor based control system which would automatically vary the shaft support dynamic characteristics in accordance with the requirements for minimising machine vibration.

In order to carry out the remainder of the research programme described above a third year of funding will be required, in accordance with the original project grant application document. With this proviso, the authors recommend that experimental testing should begin at about November 1986.

13. REFERENCES


1. M P Roach, M Goodwin — "Vibration Control In Rotating Machinery Using M J Variable Dynamic Stiffness Squeeze Films. 1st full Interim Scientific Report covering the period 1 September 1984 - August 1985". Volume 1, Submitted to EOARD September 1985.

2. R G Kirk and J Gunter — "Effect of Support Flexibility and Damping On the E Dynamic Response of A Single Man Flexible Rotor in Elastic Bearings". NASA Report No. CR2083 July 1972.

3. J W Lund & Sternlicht — "Rotor-Bearing Dynamics with Emphasis On B Attenuation". ASME J Basic Eng. December 1962.

4. E J Gunter, L E Barrett & P E Allaire — "Stabilazation of turbomachinery with Squeeze Film Dampers - Theory and Applications". I.Mech.E. Paper C233/76 1976.

5. L E Barrett, E J Gunter & P E Allaire — "Optimum Bearing and Support Damping for Unbalance Response and Stability of Rotating Machines". J Eng Power, Volume 100. January 1978.

6. M J Goodwin — "Variable Impedance Bearings for large Rotating Machinery". PhD thesis, Univ. Aston, 1981.

7. M J Goodwin, C J Hooke & J E T Penny — "Controlling the Dynamic Characteristics Of Hydrostatic Bearings By Using Pocket-Connected Accumulators". Proc. I.Mech.E.

8. A A Raimondi & J Boyd — "An Analysis of Orifice and Capillary Compensated Hydrostatic Journal Bearings". Lubrication Engineering, January 1957.

9. Pestel & Leckie — "Matrix Methods in Elasto-Mechanics". Mc-Graw Hill Book Co Ltd, 1963

10. J S Rao — "Rotor Dynamics". Wiley Eastern Ltd, 1983.

11. M J Goodwin — "Dynamics of Rotor-Bearing Systems". George Allen & Unwin. (in press).

12. H I Bush — "Some Design Details of the General Electric TF34 Turbofan Engine" Private communication.

## APPENDIX

This appendix contains a number of graphs which indicate the variation of hydrostatic bearing dynamic characteristics with changes in the design parameters pressure ratio $\beta$, clearance, oil supply pressure and land width. These graphs have been discussed in section 8.

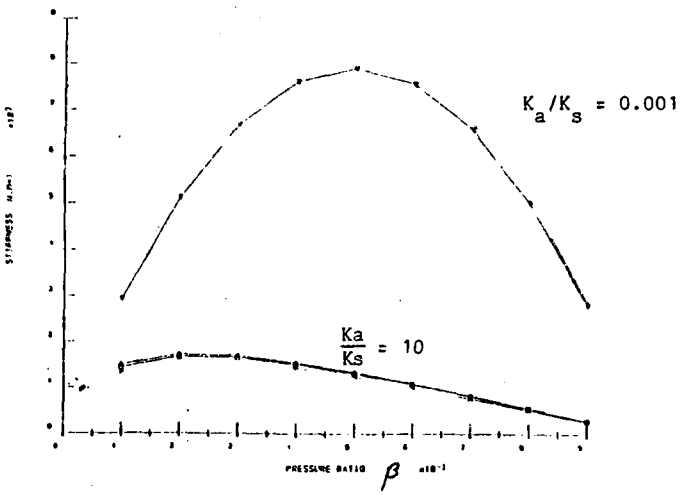


Figure 23: Variation of Bearing Stifness Coefficient $K_{yy}$ with Pressure Ratio β

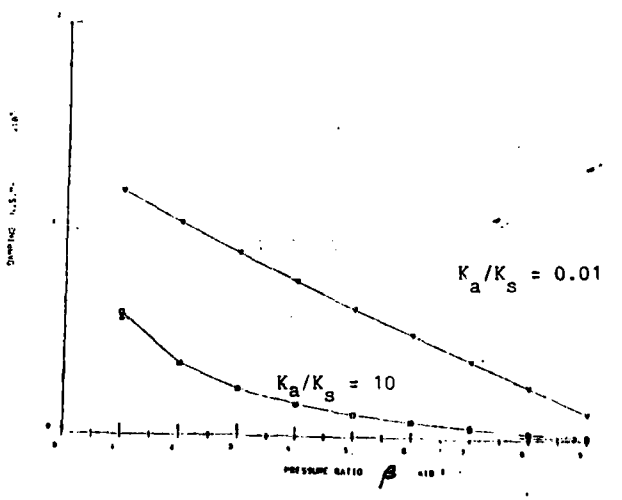


Figure 24: Variation of Bearing Damping Coefficient $C_{yy}$ with Pressure Ratio β

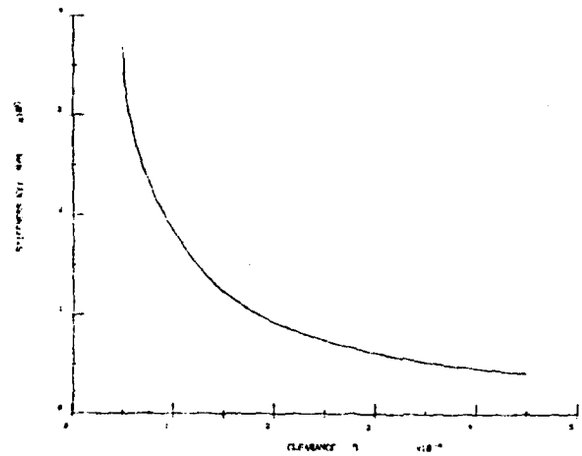

Figure 25: Variation of Bearing Stiffness Coefficient $K_{yy}$ with Clearance

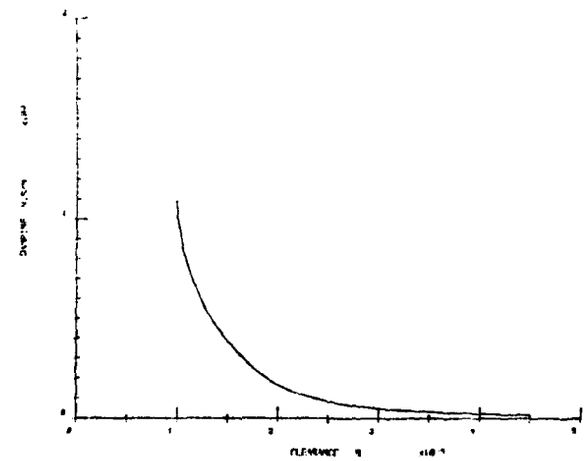

Figure 26: Variation of Bearing Damping Coefficient $C_{yy}$ with Clearance

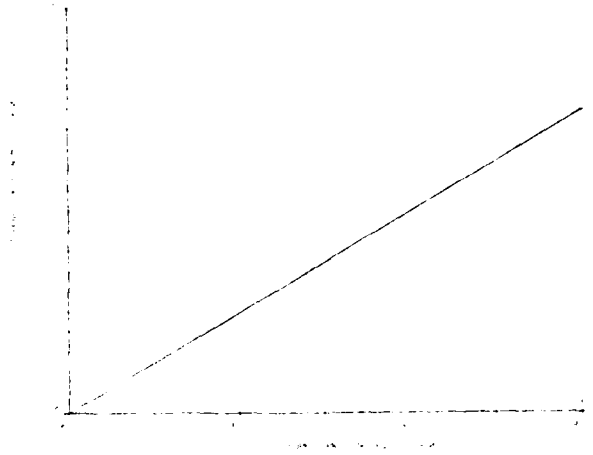

Figure 27: Variation of Bearing Stiffness Coefficient $K_{yy}$ with Supply Pressure

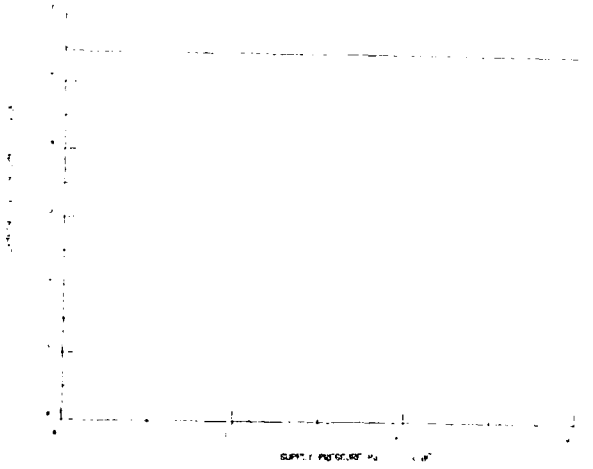

Figure 28: Variation of Bearing Damping Coefficient $C_{yy}$ with Supply Pressure

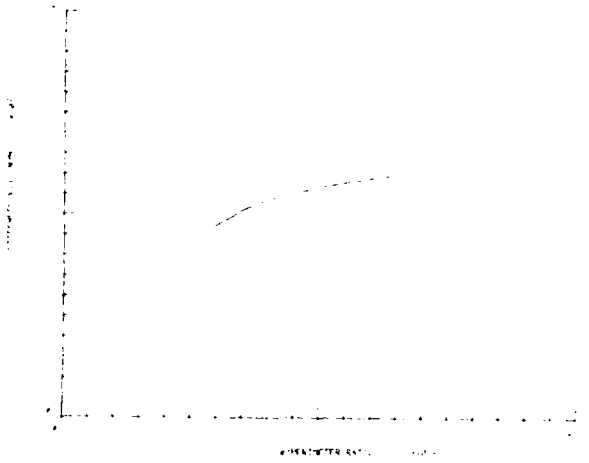

Figure 29: Variation of Bearing Stiffness Coefficient $K_{yy}$ with Ratio Land width/perimeter length

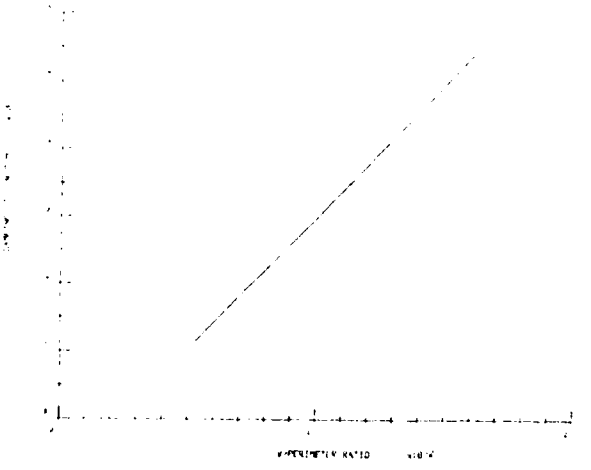

Figure 30: Variation of Bearing Damping Coefficient $C_{yy}$ with Ratio Land width/perimeter length

END

DATE
FILMED

1-87

DTIC